buildings

MDPI

Article

Investigation of the Mechanical, Microstructure and 3D Fractal Analysis of Nanocalcite-Modified Environmentally Friendly and Sustainable Cementitious Composites

Mahmoud Ziada [1], Yosra Tammam [2], Savaş Erdem [1,*] and Roberto Alonso González Lezcano [3,*]

[1] Avcilar Campus, School of Civil Engineering, Istanbul University-Cerrahpasa, Istanbul 34200, Turkey; m.ziada@ogr.iu.edu.tr
[2] Civil Engineering Department, Avcilar Campus, Istanbul Gelisim University, Istanbul 34200, Turkey; yosra.tammam@ogr.iu.edu.tr
[3] Architecture and Design Department, Escuela Politécnica Superior, Universidad CEU San Pablo, 28668 Madrid, Spain
* Correspondence: savas.erdem@iuc.edu.tr (S.E.); rgonzalezcano@ceu.es (R.A.G.L.)

Abstract: Unlike conventional concrete materials, Engineered Cementitious Composites (ECC) use a micromechanics-based design theory in the material design process. Recently, the use of nanoparticles in various concretes and mortars has increased. This study used nanocalcite to investigate the mechanical, microstructural fractal analysis of environmentally friendly nanocalcite-doped ECC (NCa-ECC). This paper investigated the effects of nanocalcite (NCa) with different contents (0.5, 1, and 1.5% by mass of binder) on the mechanical properties of engineered cementitious composites (ECC). For this purpose, compressive strength, ultrasonic pulse velocity (UPV), and flexural strength tests were conducted to investigate the mechanical properties of the ECC series. In addition, SEM analyses were carried out to investigate the microstructural properties of the ECC series. The content of nanocalcite improved the mechanical and microstructural properties of the nanocalcite-modified ECC series. In addition, the 1 NCa series (1% nanocalcite modified to the mass of the binder) had the best performance among the series used in this study.

Keywords: nanocalcite; environmentally friendly cementitious composite; mechanical properties; microstructure analysis; 3D fractal analysis; sustainability; fly ash

Citation: Ziada, M.; Tammam, Y.; Erdem, S.; Lezcano, R.A.G. Investigation of the Mechanical, Microstructure and 3D Fractal Analysis of Nanocalcite-Modified Environmentally Friendly and Sustainable Cementitious Composites. *Buildings* **2022**, *12*, 36. https://doi.org/10.3390/buildings12010036

Academic Editor: Chiara Bedon

Received: 19 November 2021
Accepted: 22 December 2021
Published: 2 January 2022

1. Introduction

Cementitious materials perform a necessary part in the construction sector and are therefore of paramount importance to improve their durability and mechanical characteristics [1–5]. Because of recent characterization technology progress, the characteristics of all these synthetic structures may be examined on a variety of length scales ranging from nano to macro [6–8]. Thus, cement materials' structure and behavior patterns at the sub-micrometer scale are better understood, which has improved their macro-properties [9]. For example, the durability can be improved by reducing the cement paste's total porosity by inserting additives in a range of pores primarily present at a micrometer length scale [10–12]. The studies performed on environmentally friendly and sustainable composites recently have gained importance. Tosee et al. [13] investigated the compressive strength of environmentally friendly concrete modified with eggshell powder using the hybrid ANN-SFL optimization algorithm. They found that the highest compressive strength was obtained for the samples containing 7–9% of eggshell powder and it was 55% higher than their control samples. Ziada et al. [14] produced environmentally friendly fly ash-based and basalt powder waste-filled sustainable geopolymer mortar with basalt fiber. They found that the produced sustainable mortar had high strength and durability properties and the use of 1.2% of basalt fiber increased samples' compressive strength by up to 18%

and flexural strength by up to 44%. Şahmaran et al. [15] produced ECC mixes with various FA/PC ratios (1.2, 2.2, and 4.2). They found that the increase of FA content in ECC specimens exhibit more ductile behavior.

Ultra-high-molecular-weight polyethylene, carbon, and high-modulus polyvinyl alcohol (PVA) fibers are now used in cement-based products. PVA fibers are widely used because the first two fibers are too costly to be commonly used [16–18]. The modification of fibers in cement-based materials focuses on increasing toughness [19,20]. Overall, using fiber improves interfacial adhesion. However, this enhances the bridging result between such fiber and the interface, and it overlooks the influence of sliding friction on fracture energy. When fibers are detached, the increased bond strength at the interface causes a large amount of fracture energy to be generated quickly, raising the potential of brittle fracture [21]. Previous articles had improved the toughness of concrete by altering the content of cementitious composites, such as micro compounding, in which certain microscale particles are added to the concrete mix to increase the toughness of the concrete [22,23].

Unlike conventional concrete materials, Engineered Cementitious Composites (ECC) use a micromechanics-based design theory in the material design process. In a single tensile loading, PVA-ECC has tight and multiple cracking behaviors. The intrinsically cracking width of less than 100 mm is high ductility and improved durability [24]. The tensile strain capacity for PVA-ECC over five percent was demonstrated using commonly available materials and equipment in the concrete manufacturing sector [25]. Li et al. [26] found that the fiber volume should not be more than 2% to ensure good performance in ECC blends. Due to their composite performance and economic considerations, PVA fibers are among the types of fibers used by ECC and the other high performance cementitious composites [27–31].

Nanomaterials have been demonstrated to enhance the interfacial transition area of structures by speeding up the hydration reaction, considerably improving the porosity and durability of the hardened cement-based mixtures [32]. Furthermore, the addition of nanoparticles generally increase the matrix fracture toughness due to the shielding effect on the crack tip and improves the multiple cracking behavior of engineered cementitious composites by making the fiber distribution more homogenous [25]. Among the nanoparticles, nano-$CaCO_3$ is one of the most used nanoparticles in cementitious composites [33]. The most stable shape of naturally abundant inorganic Calcium Carbonate ($CaCO_3$) material in nature is nanocalcite. Calcium Carbonate ($CaCO_3$) is immaculate, crystalline, and highly transparent. Nanocalcite offers advantages in addition to its excellent functions, such as enhancing resilience and rigidity, providing perfect stability and insulation in electricity.

The fracture surface morphology of cementitious materials resulting from crack propagation under loading would explain the differences in the mechanical behavior and the corresponding failure mode [34,35]. It is well established that several parameters control the roughness and texture of the fracture surface of the cementitious composite. The meandering of main crack (for example, tortuous or much less tortuous fracture surfaces) is considerably influenced by the use of micro and nano additives, properties of aggregate particles, and the concrete mix design [36]. Beginning with the pioneering work by Mandelbrot [37], the concept of fractal geometry and fractal dimension has become popular in construction technology and associated materials to better understand the relationship between the flexural response and the tortuosity of fracture surface in ECC [33] and for the design multiscale reinforcing fibers of composite materials [38].

The literature review above clearly indicates that research in this field has generally focused on evaluating strength properties, durability-related behavior, and thermomechanical performance at a macro level. However, research conducted thus far is still less to comprehensively evaluate the microstructure-associated mechanical and fracture characterization of engineered cementitious mixes modified with nanocalcite and 3D fractal characterization. This leads to the aim of this study, which is to analyze the mechanical performance and micro-structural damage characteristics of nano-modified ECC mixes and to improve the toughness, the multiple cracking behavior and the strength of the strain

hardening ECC composites for the development of super infrastructures, which are driven to attain higher strength and higher toughness. In this study, the effects of nanocalcite on ECC's mechanical and microstructural properties are investigated by modifying nanocalcite with 0%, 1%, and 1.5% mass of binder. Compressive strength, flexural tensile strength, and ultrasonic pulse velocity (UPV) tests were performed to investigate nano-modified ECC mixtures' mechanical and physical properties. In addition, scanning electron microscopy (SEM) and 3D fractal analysis were performed to examine the microstructural and crack analysis of the samples.

2. Materials and Methods

2.1. Materials and Mixing Procedures

CEM I 42.5N Portland cement, fly ash (Class F), silica sand, water, high-range water-reducing admixture (HRWRA), and polyvinyl alcohol (PVA) fibers were used to prepare the ECC samples. The chemical and physical properties of the binder (Portland cement and fly ash) and filler (silica sand) are listed in Tables 1 and 2, respectively. In addition, the mixing ratios of the blends are listed in Table 3. Ding et al. [39] replaced the NCa material with Portland cement by 0%, 1%, 2%, 3% ratios to obtain nano-$CaCO_3$ modified ultra-high performance engineered cementitious composites mixes. In this study, the NCa was replaced with the binder by 0%, 0.5%, 1%, 1.5% ratios. Figure 1 shows the used nanocalcite materials and PVA fibers. In the mixing phase, the Portland cement (PC), fly ash (FA), and silica sand were dry blended for 3 min in a mixer. After that, HRWRA and dissolved water were added and mixed for another 5 min. Then, PVA fibers were added into the fresh mortar until it was homogeneous. Finally, nanocalcite was added with 0.5, 1, and 1.5 ratios and mixed homogeneously. The nanocalcite used in this study is white, with a purity of 99.9% and an average particle size of 900 nm. The freshly prepared mixture was poured into 15 × 50 × 350 mm molds and 50 × 50 × 50 mm cubic molds, and then these molds were covered with a plastic sheet. The specimens were cured at 23 °C. Figure 2 shows poured fresh nanocalcite-doped ECC samples.

Table 1. Chemical properties of binder and filler materials (% by weight).

Binder and Filler Materials Used	Na_2O	K_2O	MgO	CaO	Fe_2O_3	SiO_2	Al_2O_3	LOI
FA	0.7	1.9	1.7	3.5	5.5	61.1	21.8	1.58
PC	0.2	0.8	2.5	61.3	3.34	20.80	5.50	2.22
Sand	0.021	0.011	0.011	0.022	0.022	99.80	0.062	0.075

Table 2. Physical properties of binder and filler materials.

Binder and Filler Materials Used	Specific Gravity	BF (m^2/kg)
FA	2.11	292
PC	3.065	326
Sand	2.65	-

Table 3. Mixture ratios of nanocalcite-doped ECC series.

Mixture ID.	PC	W/B [1]	PVA (vol.%)	FA/PC	NCa/B [1] (%)	Sand/PC	HRWRA (kg/m^3)
0 NCa	1	0.25	2	1.25	-	0.82	5.50
0.5 NCa	1	0.25	2	1.25	0.5	0.82	5.55
1 NCa	1	0.25	2	1.25	1	0.82	5.60
1.5 NCa	1	0.25	2	1.25	1.5	0.82	5.65

[1] B: Binder materials (PC + FA).

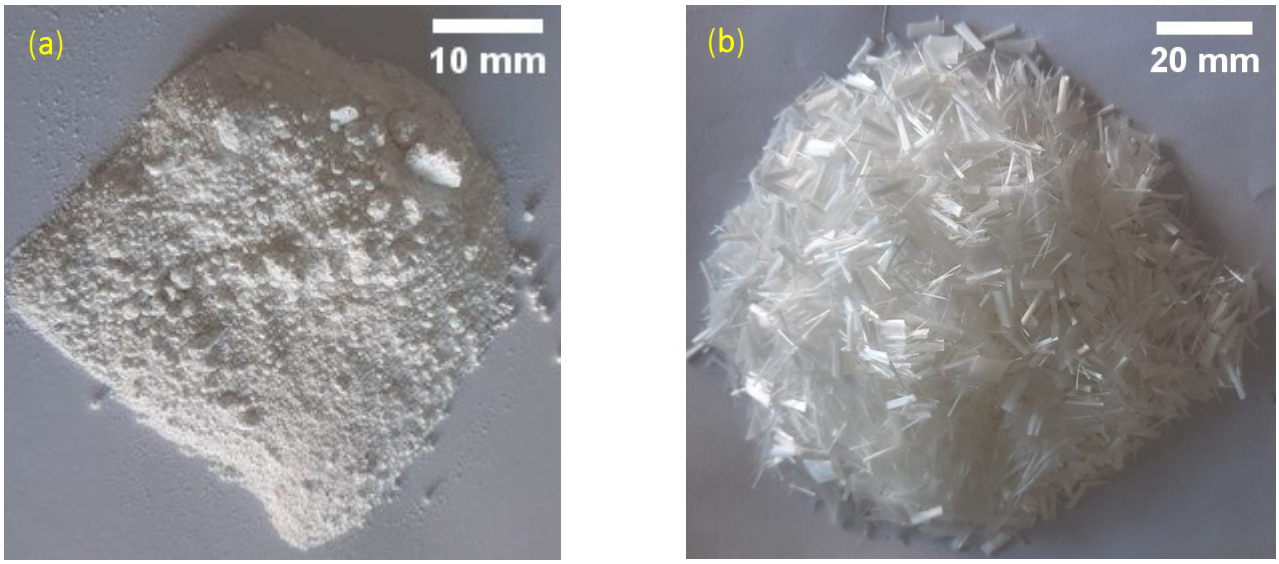

(**a**) (**b**)

Figure 1. (**a**) Nanocalcite materials (**b**) PVA fiber.

Figure 2. Poured fresh nanocalcite-doped ECC samples.

2.2. Performed Tests and Specimens

In this study, compressive strength, flexural strength, and UPV tests were performed on NCa-ECC specimens. Then, 3D fractal analysis was conducted. Finally, the microstructure of the specimens was investigated using SEM analysis. First, the ultrasonic pulse velocity (UPV) was tested according to ASTM C 597 to determine the UPV values of three 50 × 50 × 50 mm cube samples for each series after 28 days [40]. Then, 50 × 50 × 50 mm cube specimens were placed in a compressive strength testing machine with a capacity of 2000 kN and subjected to compression at a rate of 0.602 MPa/s. Factors such as loading speed, size, and age of the samples were entered into the pressure machine before loading to obtain compressive strength values automatically. Thus, the compressive strength test was performed on three cubes of each series according to ASTM C109 [41]. The flowability of the fresh mixtures was tested according to ASTM C230 [42]. The spreading diameter of the mixtures obtained from this experiment was equal and measured approximately 210 mm. Thus, the fresh mixtures given in Table 3 showed good fluidity without segregation.

In this study, the flexural strength test was performed on 15 × 50 × 350 mm samples to obtain flexural strength, mid-span displacement, strain, and stress-deflection curves according to ASTM C348 [43]. For this proposal, a closed-loop controlled universal testing machine (Figure 3) with a loading rate of 0.003 mm/s was used. Three samples were used for each series, and the average results of the samples were obtained. The flexural stress-deflection curves were obtained using flexural strength values and deflections, recorded by the computer data recording system on the testing machine. Erdem and Gurbuz [44] performed a similar test on hybrid fiber reinforced engineered cementitious specimens.

Figure 3. The flexural test set-up.

Figure 4 shows the multiple cracks formed in the samples subjected to the flexural strength test. The crack of the prismatic sample was obtained using a 40× magnification microscope to observe the PVA inside the crack. Figure 5. shows the crack of the sample subjected to the flexural test at 40× magnification. After the strength tests, small pieces of the specimen were taken and subjected to SEM. The microstructure of the samples was studied using SEM analysis.

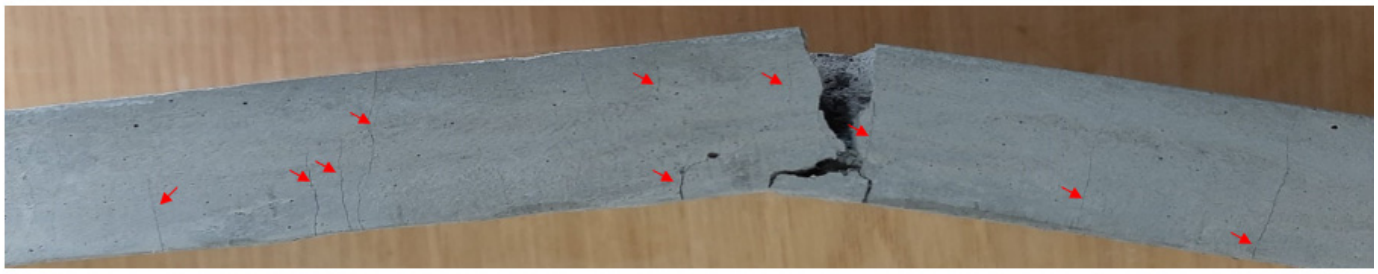

(**a**)

Figure 4. *Cont.*

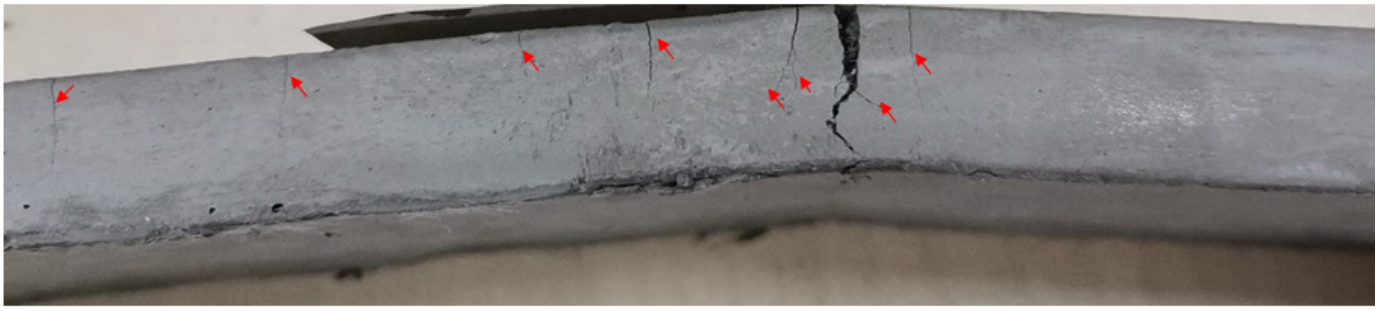

(**b**)

Figure 4. The specimens were subjected to the flexural strength test. (**a**) 0 NCa; (**b**) 1 NCa.

Figure 5. The appearance of a crack in a specimen subjected to the flexural test at 40× magnification.

In addition, following the flexural tensile tests, the fractal dimensions of cracks were determined. Images of the samples after the flexural testing were firstly captured using a high-resolution camera. Then, these images were converted from RGB mode to an 8 bytes greyscale and scaled up to reflect the actual dimensions. The main flexural bending moment-induced cracks at the same point for all the samples were digitized for thresholding using open-access digital image analysis software called Image J. Then, these were covered by imaginary meshes with rectangular box sizes containing the number of pixels of the crack image (Figure 6). Next, the number of grid squares to cover the cracks was counted for the plot of In (box count) versus In (box size), which were used to compute the average value of fractal dimension that is the slope of the line joining the logarithm of the number of grid squares encountered by the crack and the logarithm of the square grid dimension.

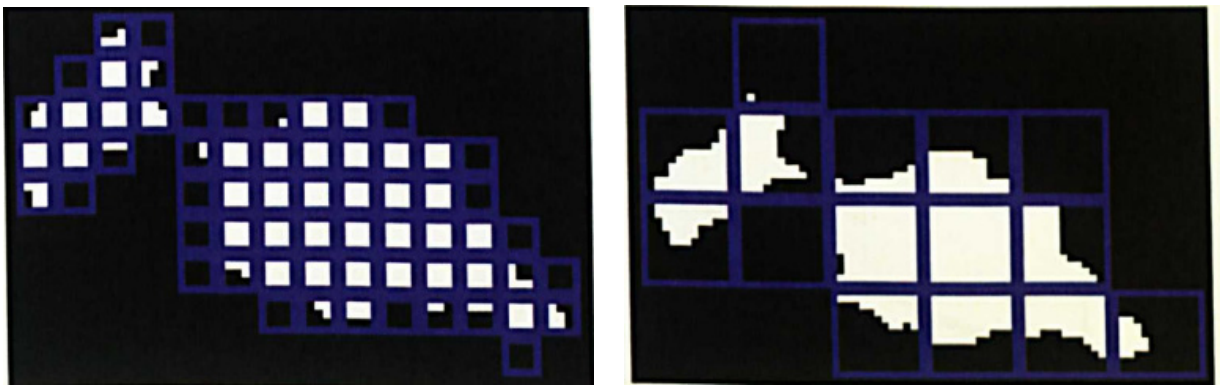

(**a**) (**b**)

Figure 6. Example of crack analysis with different box sizes using Image-J software. (**a**) Boxing size of 1 unit (**b**) Boxing size of 4 unit.

Then, using the formula established by Guo et al. [45], the composites' dissipated fracture energy (Ws/Gf) was approximated at the macro scale as a function of the surface macro-cracks. The ratio of energy (Ws) produced by crack propagation to fracture energy (Gf) is shown by the value of Ws/Gf.

$$Ws/Gf = a \times (\delta/a)\, D^{1-d} \quad (1)$$

where a denotes the Euclidean length (equal to the diameter of the tested composite), and D^{1-d} denotes the fractal dimension of the crack.

3. Results and Discussion

3.1. Compressive Strength and Ultrasonic Pulse Velocity (UPV) Results

The compressive strength and UPV tests after 28 days of the fabricated series with three different ratios of nanocalcite are shown in Figures 7 and 8. Compressive strength results were obtained by averaging three 50 × 50 × 50 mm cubic samples for each series. The maximum increase in compressive strength and UPV values were obtained for 1 NCa (1% by mass of binder) specimens. When the NCa content was increased from 0.5 to 1 percent, the compressive strength of NCa-ECC increased steadily by 2.17 to 6.92 percent compared to the 0 NCa series. When the NCa content was increased to 1.5 percent, the enhancement of compressive strength decreased to 4.64 percent. The increased strength could be attributed to both the filling effect and the chemical effect associated with NCa. NCa can react with C3A to form mono-carbonate, which has a unique structure with strong hydrogen bonds between oxygen atoms and interlayer waters in carbonate groups [46]. In addition, $CaCO_3$ can increase the stability and nature of ettringite [47]. The difficulty of uniform distribution may be the reason for the less apparent positive effect of NCa at higher dosage on compressive strength [39]. As a result, increasing the nanocalcite content in the mixes increased the compressive strength values. These increases were 50.17, 51.26, 53.64, and 52.50 MPa for 0, 0.5, 1, and 1.5 NCa series. When the content of Nano-$CaCO_3$ increased from 1% to 1.5%, the improvement of strengths was reduced. Because excessive NCa addition led to poor dispersion of the matrix, insufficient hydration, and limited the improvement of the strength of the samples [48]. In addition, The matrix had an agglomeration effect due to the increase of nano-materials. In addition, free water cannot reach the cement particles, which reduces hydration and reduces the strength of the concrete [49].

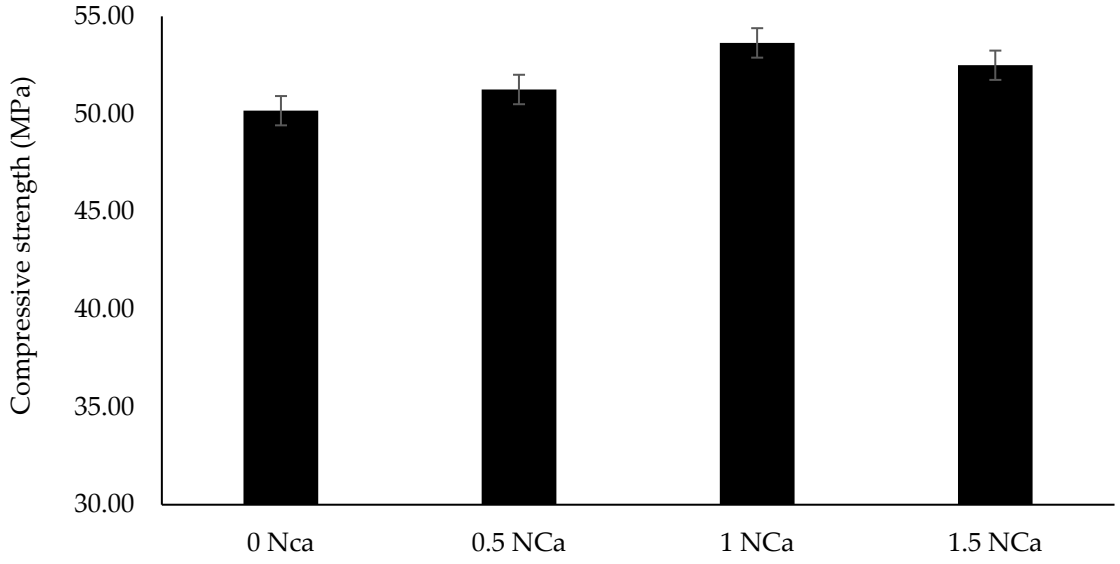

Figure 7. Compressive strength results of NCa-ECC.

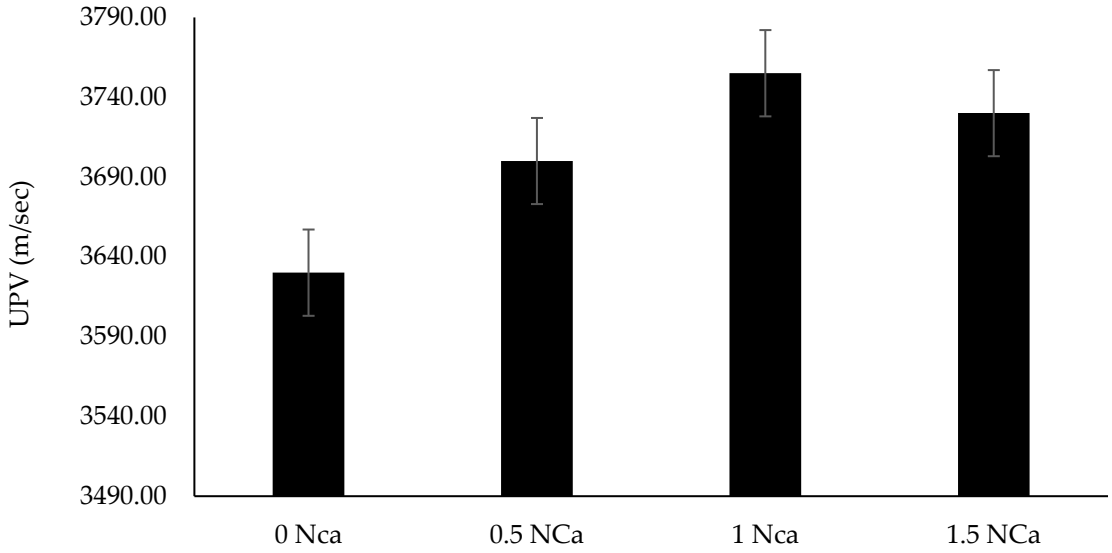

Figure 8. UPV results of NCa-ECC.

Figure 8 shows the ultrasonic pulse velocity (UPV) testing of NCa-ECC samples with different mixtures. Looking at the UPV results, it is observed that the result has a parallel relationship with the compressive strength results. The UPV increased with increasing nanocalcite content in the mixes by 3630.06, 3700, 3755, and 3630 m/sec for 0, 0.5, 1, and 1.5 NCa series. Adesina and Das [50] investigated the UPV values of 50 × 50 × 50 mm cubic ECC samples by replacing crumb rubber with silica sand. They found that the UPV value of ECC samples without adding crumb rubber was 3689 m/s, while the UPV value decreased to 2976 m/s when they used 100% crumb rubber. The UPV result of ECC without the addition of crumb rubber obtained in their study was consistent with the UPV result of the ECC without the addition of NCa obtained in this study. In addition, the correlation between compressive strength and UPV for all the mixes is shown in Figure 9. Figure 9 shows that the R coefficient is 0.9264. This R coefficient indicates a strong relationship between UPV and the compressive strength of the specimens.

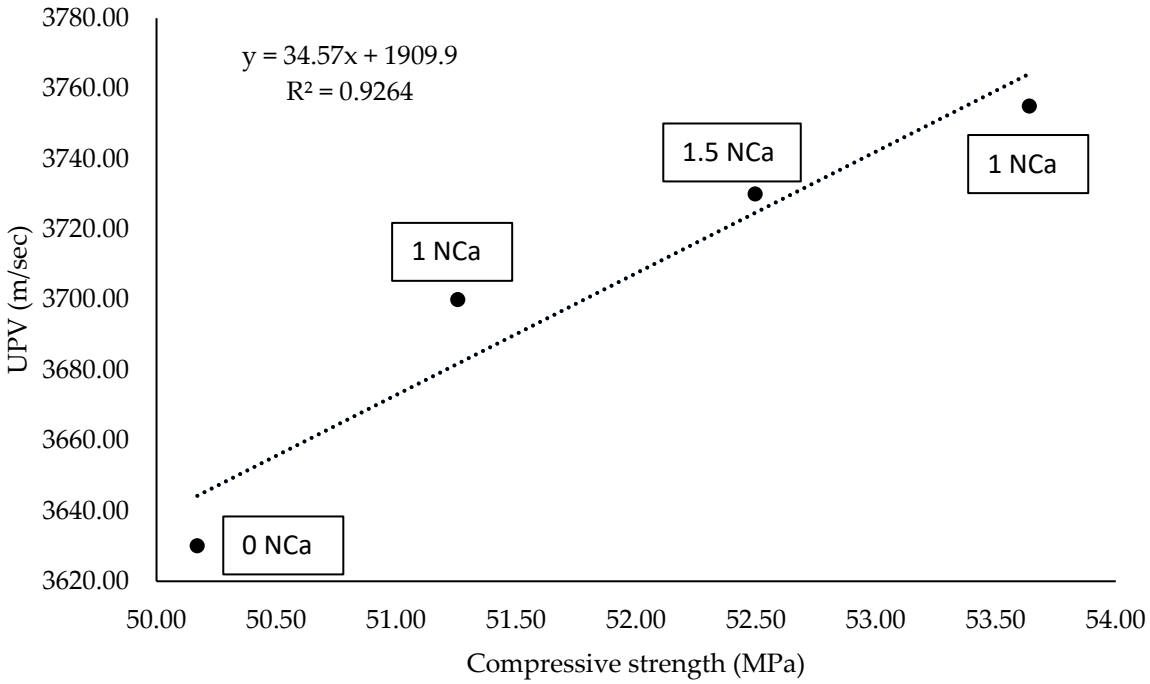

Figure 9. Correlation between compressive strength and UPV.

3.2. Flexural Performance

Test results of 15 × 50 × 350 mm specimens subjected to flexural test after 28 days are shown in Figure 10. The results were obtained by averaging the flexural results of three samples for each series. The maximum increase in flexural strength was obtained for 1 NCa specimen. Accordingly, the increase in the nanocalcite content in the mixes increased the flexural strength values. Sun et al. [51] found that the content of nano-$CaCO_3$ improved the flexural performance of ECC. In addition, increasing the nanocalcite content in the blends increased the flexural strength values to 13.1, 14.31, 16.9, and 15.31 MPa for 0, 0.5, 1, and 1.5 NCa series, respectively. In general, the increase in the flexural strength values with the addition of the nanomaterials would be further beneficial for applying ECC-steel bar reinforced composite beams. In this case, the ECC with higher flexural strength could carry developing tensile stress under flexural loading and the steel reinforcement rebar after cracks. This, in turn, results in a much higher load-carrying capacity for the composite.

Moreover, mid-span displacement, strain, and stress-deflection curves were obtained from the flexural strength test. The strain, mid-span displacement, flexural toughness, and ductility index results obtained from the stress-deflection curves are shown in Table 4. This table indicates that 1 NCa samples have the highest strain and mid-span displacement values. Thus, the increase in the content of nanocalcite increased the flexural performance and compressive strength of the samples. In addition, by examining the stress-deflection curves of 15 × 50 × 350 mm specimens shown in Figure 11, the content of NCa improved the flexural performance. The maximum deflection values (deflection capacity) of the samples subjected to the flexural strength test were obtained from the endpoints of the flexural stress-deflection curves. The increases in the deflection capacity of the 0.5 NCa (11.74 mm), 1 NCa (12.88 mm), and 1.5 NCa (12.51 mm) series were 46.70%, 61.01%, and 56.39%, respectively, compared to the 0 NCa (8 mm) series. Furthermore, the flexural strength increases of 0.5, 1, and 1.5 NCa series were 8.68%, 31.55%, and 18.68, respectively, compared to the 0 NCa series. Thus, series 1 NCa exhibited the best flexural properties, having the highest flexural stress and deflection values. Ding et al. [39] found that the content of nano-$CaCO_3$ increased the strength of UHP-ECC, and an NC content of three percent (by mass of cement) was considered ideal. In their study, they replaced the NC material with PC only, but if they had replaced the NC material with a binder (FA and PC),

the ratio they used would have been approximately 1–1.5% by mass of the binder. Thus, their conclusion was close to the conclusion of this study.

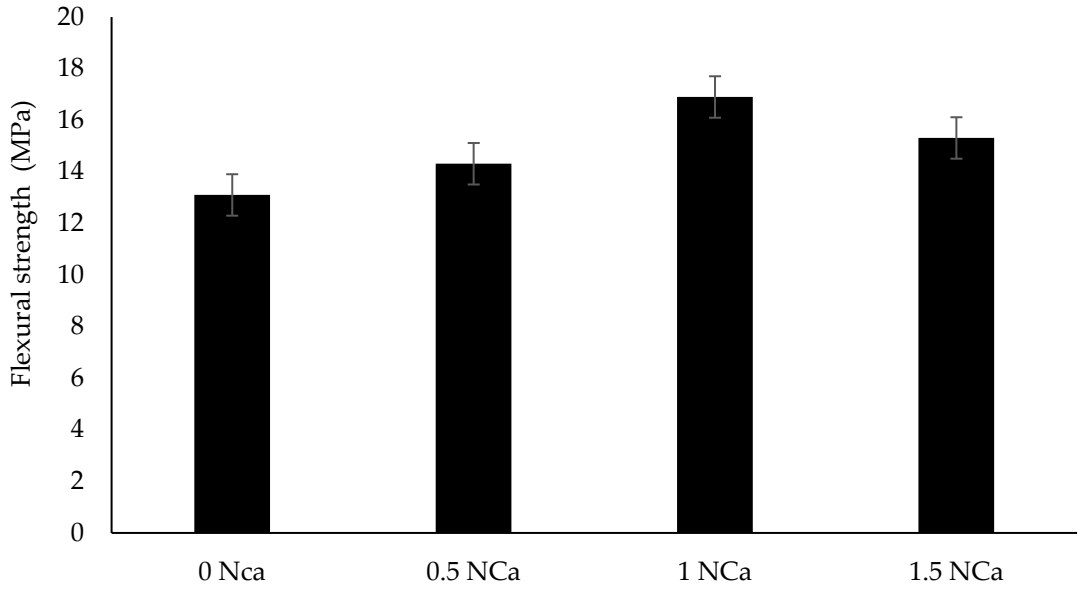

Figure 10. Flexural strength results of NCa-ECC.

Table 4. Strain, mid-span displacement, flexural toughness, and ductility results.

Mix ID	0 NCa	0.5 NCa	1 NCa	1.5 NCa
Mid-span displacement (mm)	3.50	3.48	8.45	5.57
Strain (%)	0.39	0.38	0.84	0.56
Flexural Toughness (MPa.mm)	74.7	75	161	99.2
Ductility index increase (%)	0	0.21	98.20	39.44

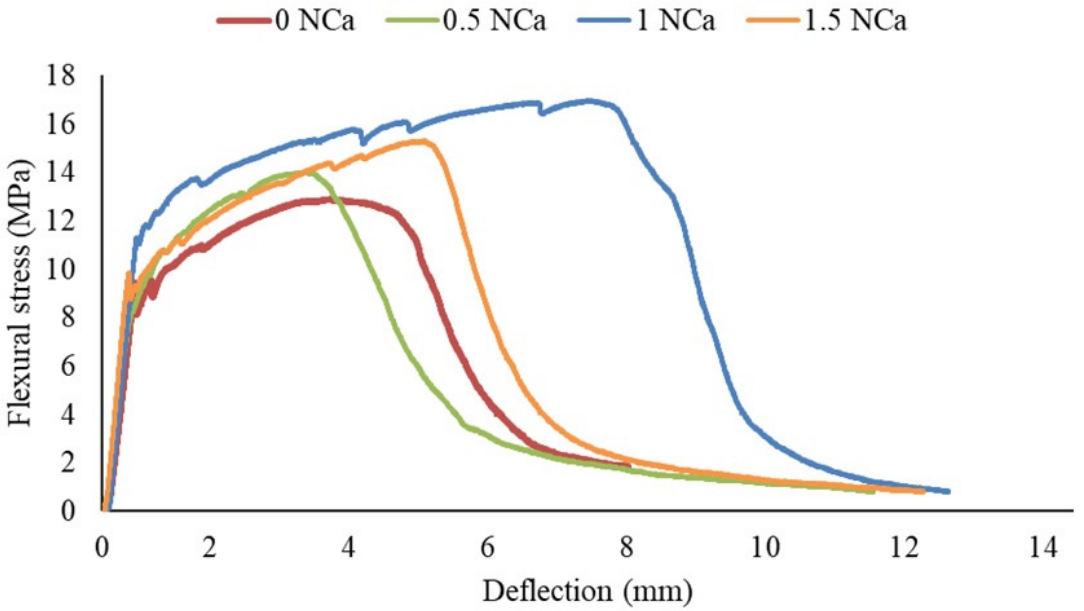

Figure 11. Flexural stress–deflection curves of the specimens.

Ductility and flexural toughness can be evaluated using flexural load-deflection curves, as indicated in the literature [52,53]. The area under the whole load-deflection curve is used

to compute flexural toughness, and the load–deflection curves were also used to calculate ductility. The ductility index (μ) calculated using the formula;

$$\mu = \delta u / \delta y \quad (2)$$

where δu is the ultimate displacement and δy is the yield displacement. After calculating the ductility indexes of the samples, the percent increases of the ductility indexes of the samples compared to the 0 NCa series were calculated and given in Table 4. NCa-containing mixtures exhibit considerably greater deflections in the ultimate state and higher loads when compared to the 0 NCa mixture. This results in a greater area under the load-deflection curves, which may indicate increased toughness. In addition, it can be concluded that adding NCa to the ECC mixes improves the ductility and flexural toughness of the mixes. In this study, the highest flexural toughness and ductility were obtained for 1 NCa specimen. Yeşilmen et al. [54] used nano-silica and nano-$CaCO_3$ in ECC mixtures, and they found that the nano- $CaCO_3$ contained ECC mixtures had the highest ductility. The higher fracture toughness and improved multiple cracking behavior associated with the nano-particle reinforced mix can make ECC effectively improve the unstable crack propagation caused by the surrounding concrete or old/new concrete interface. This, in turn, reduces the common early damage types in repair structures such as spalling and interlaminar fracture [55].

3.3. Fractal Analysis

In the literature, there are various methods (cube counting, variance methods, etc.) for extracting and then calculating the cracking map and fractal dimension of surface cracks at the fractured 15 × 50 × 350 mm samples shown in Figure 12. Box-counting is the most preferred and practical technique for measuring the borders of a form by measuring the distances between points on it using square boxes. Erdem and Blankson [36] described the techniques in depth in prior research.

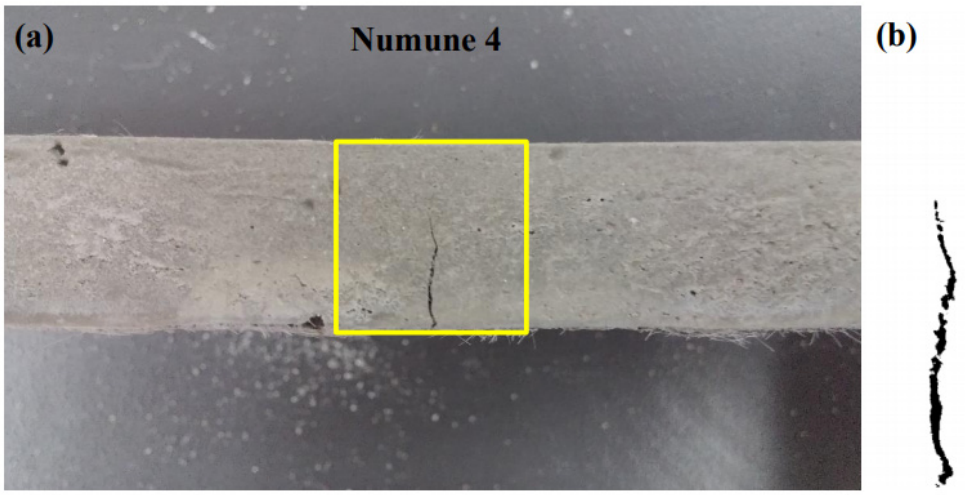

Figure 12. (**a**) An example of the crack on the studied sample (**b**) the extracted map of the crack.

The fractal dimension values of the surface cracks provided by the Image J program are illustrated in Figure 13. The results clearly show that the ECC mix with 1% nanocalcite particles (1 NCa) has the highest fractal dimension value among the NCa-ECC series. In addition, the other nanocalcite dopped ECC samples had a fractal dimension higher than the control ECC series (0 NCa). The greater fractal dimension of the 1 NCa mixture resulted in higher fracture energy dissipation at the macro scale level, as verified by the findings shown in Table 5. The greater fractal dimension values with the adding nanoparticles most likely indicate that the filling effect of nanocalcite particles refines the pore structures and

reduces unsaturated bonds, resulting in improved bondability between and creating the deformation hardening method along the fracture front and voids. However, using more than 1% nanocalcite particles decreases fractal dimension and fractural energy. In general, the previous studies [37,55] show that the fractal of general cementitious materials has a value of 1 and 2. The results of this study are consistent with the existing literature.

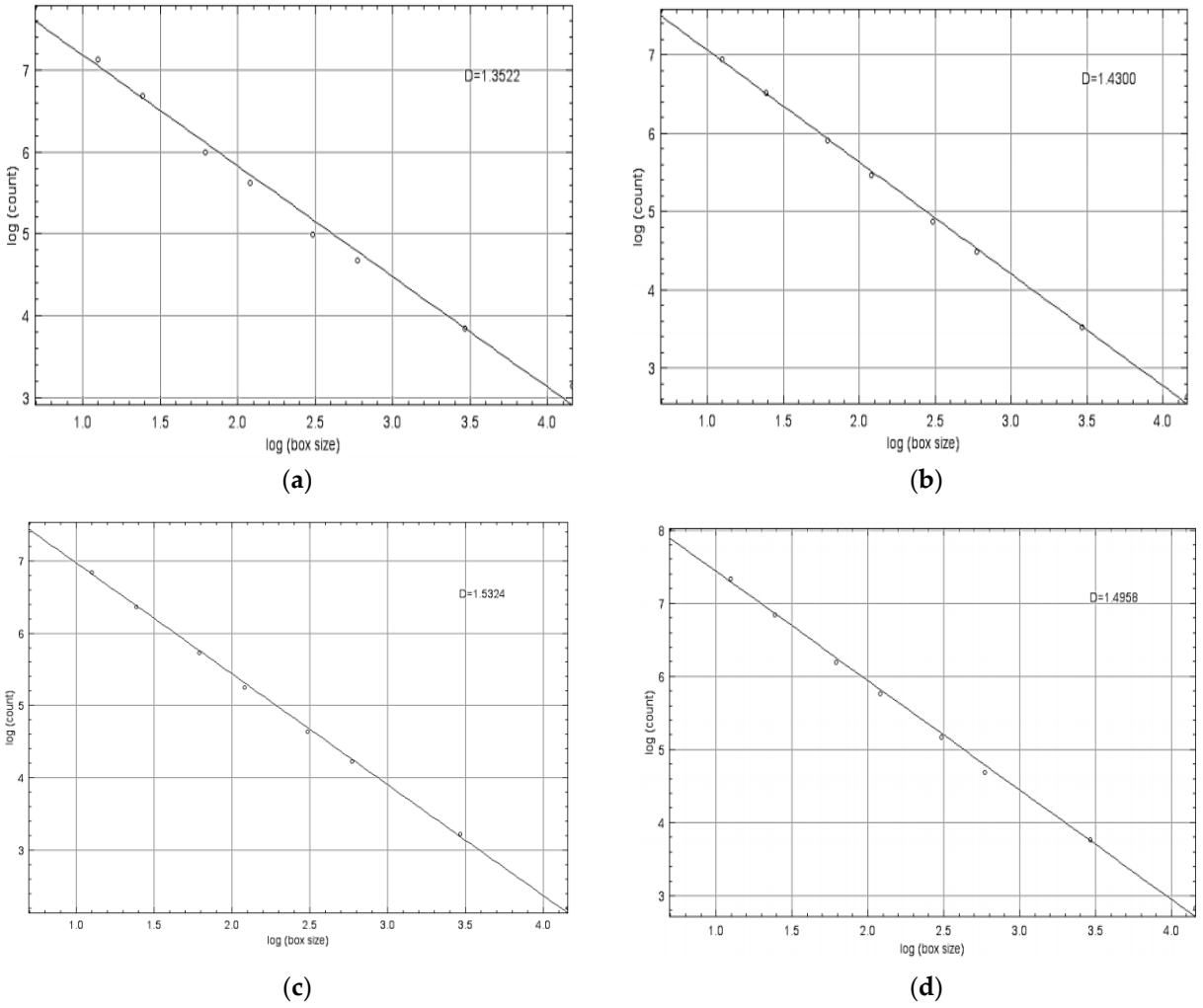

Figure 13. Fractal dimensions of the (**a**) 0 NCa, (**b**) 0.5 NCa, (**c**) 1 NCa, and (**d**) 1.5 NCa samples.

Table 5. The summary of the fractal analysis of the mixtures.

Mix ID	Fractal Dimension -D	Ws/Gf (mm)
0 NCa	1.352	113.58
0.5 NCa	1.430	158.68
1 NCa	1.532	246.40
1.5 NCa	1.495	210.53

Figure 14 illustrated 3D views of the cracked surfaces' crack surface roughness. According to the findings, the sample containing 1% nanocalcite particles had the greatest energy value during fracture initiation and propagation. The 3D surfaces curves of the mixtures corresponding with the depth of the sample locations are shown in Figure 14. The findings showed that the more fibers associated with, the larger surface area would be available to bridge cracks during the crack propagation process under flexural loading. This would, in turn, result in much higher fiber bridging complementary energy in terms

of the micromechanical principles. In general, the strong bridging ability could confirm the excellent deflection capacity with the increase in the content of the NCa particles.

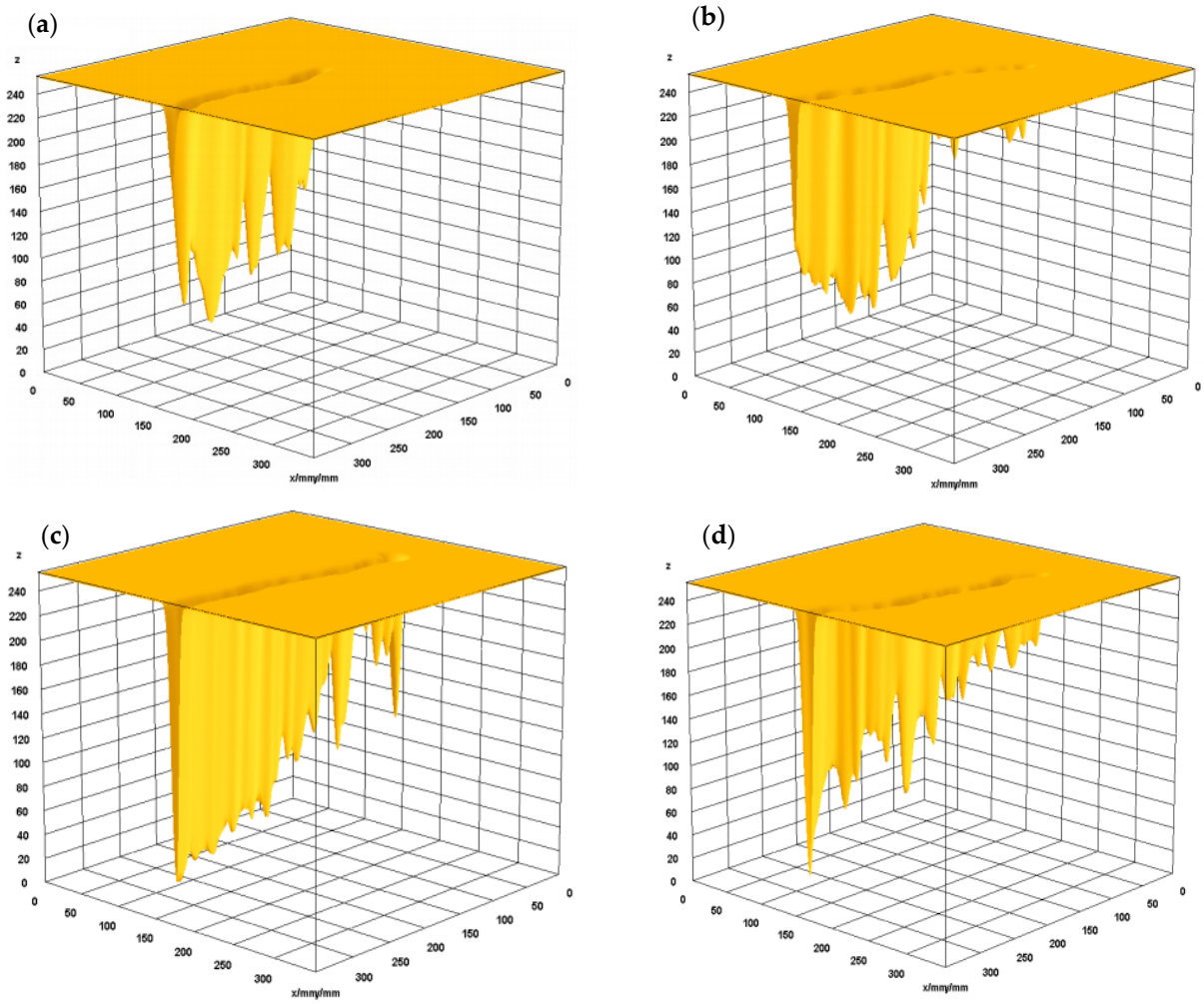

Figure 14. 3D surface graphs of the fracture surfaces of the (**a**) 0 NCa, (**b**) 0.5 NCa, (**c**) 1 NCa, and (**d**) 1.5 NCa samples.

3.4. SEM Analysis

The ECC matrix without nanomaterials is shown in Figure 15. The micrograph in Figure 15 indicates that the composites were relatively loose, with unhydrated fly ash particles clustered with distinct interfaces. It consists of dense calcium silicate hydrate (CSH) gel, unhydrated FA particles, amorphous and crystallized calcium hydroxide (CH). The micromorphology of a modified ECC sample matrix with nanocalcite (1 NCa) is shown in Figure 16. The matrix compactness improved after nanomaterials were added, and although unhydrated fly ash particles were retained, their distribution was uniform and had no clear interfaces. The main explanation for this was that the nanoparticles have a similar particle size to hydrated calcium silicate [56]. In addition, the newly formed hydration products slightly increased the density of the matrix, which improved the mechanical properties.

Conversely, the matrix did not exhibit visible micro-cracks. This, in turn, indicates that the addition of NCa particles can increase the fracture toughness of the matrix. The improvement of the matrix fracture toughness would be attributable to the shielding effect on crack tips [57]. As found in the Due et al. [58] study, the active ingredients of FA in 28-day samples prepared in this study reacted together with $Ca(OH)_2$. This reaction effectively improves the growth rate of matrix strength and imparts good strength to NCa-ECC.

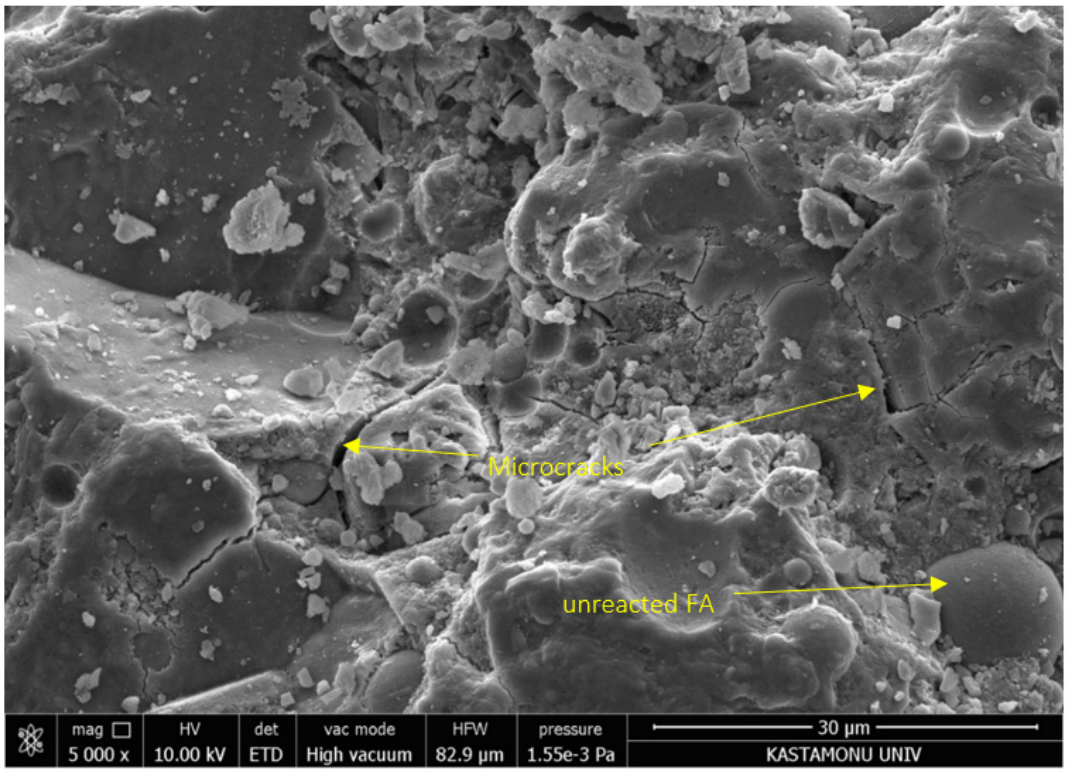

Figure 15. SEM of the 0 NCa sample magnified at 5000 times.

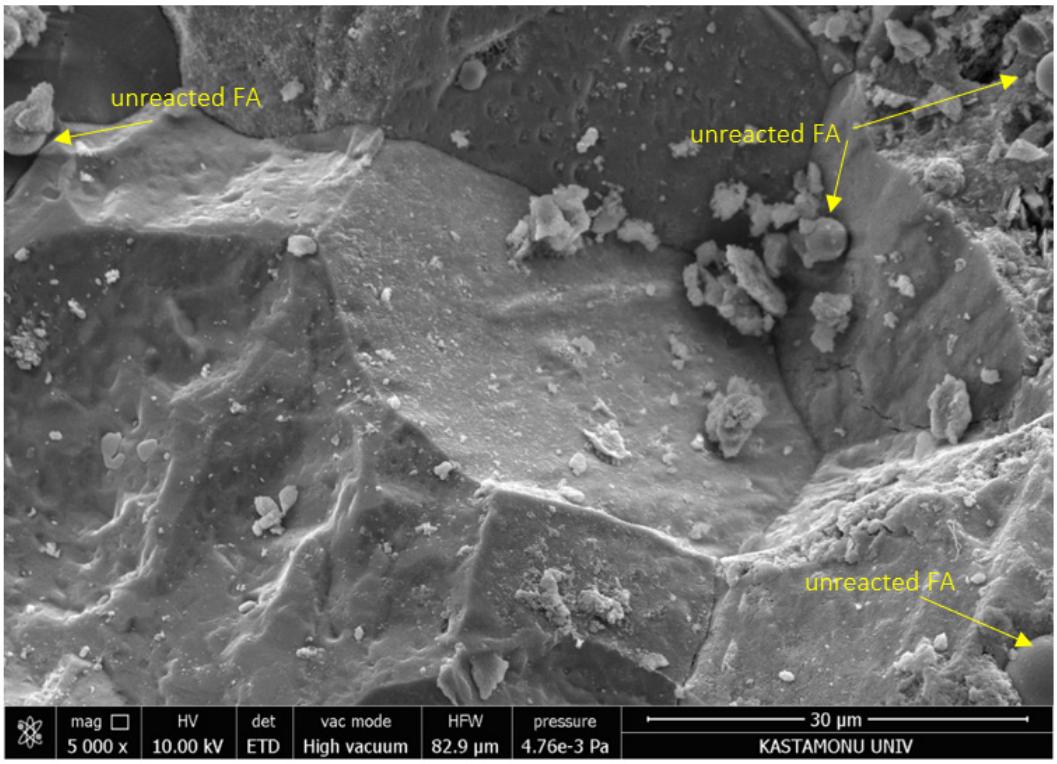

Figure 16. SEM of the 1 NCa sample magnified at 5000 times.

4. Conclusions

In this study, NCa-ECC blends were prepared by replacing 0.5, 1, and 1.5 proportions of nanocalcite in the binder of the prepared blends. Compressive strength, flexural strength, and UPV tests were carried out to investigate the mechanical properties of the NCa-ECC mixes. In addition, SEM analyses were carried out to investigate the microstructural properties of the specimens. As a result of these tests, the following results were obtained:

- Increasing the nanocalcite content in NCa-ECC mixtures increased the compressive strength. The increase in compressive strength was 2.17%, 6.92%, and 4.64% for 0.5, 1, and 1.5 NCa, respectively, compared to the 0 NCa blend.
- The increase in nanocalcite content in NCa-ECC blends increased flexural strength values. The increase in flexural strength values was 9.24%, 29.01%, and 16.87% for 0.5, 1, and 1.5 NCa, respectively, compared to the 0 NCa blend.
- Increasing the nanocalcite content in NCa-ECC blends increased the UPV. The increases in UPV were 1.93%, 3.44%, and 2.75% for 0.5, 1, and 1.5, respectively, compared to the 0 NCa blend.
- The use of nanocalcite increased the fractal dimension of the NCa-ECC samples. These increases were 5.77%, 13.31%, and 10.57% for 0.5, 1, and 1.5 NCa, respectively, compared to the 0 NCa blend.
- In general, the nanocalcite content improved the mechanical and microstructural properties of NCa-ECC mixtures.
- The addition of nanocalcite particles into the ECC mixes can increase the compressive strength. Adding more NCa particles seems to have had a negative effect on enhancing the compressive strength due to poor dispersion and a more significant air-entraining effect beyond some limit. In this experimental work, adding 1% of NCa can obtain the optimal quasi-static compressive strength.
- The deflection capacity under flexure of the ECC mixes had a significant increase after adding the NCa particles. Moreover, the strain hardening behavior associated with multiple cracks was enhanced after adding the NCa particles. Based on this experimental work, the NCa is suitable for improving the strain hardening behavior of the ECC mixes.
- This study enables producing the high toughness and high strength ECC products with the nano-particle inclusion. Nanomodified ECC, with larger Poission's effect than concrete, may be used in concrete-filled-steel-tube column that decrease the imperfect interface bonding between concrete and steel, and to produce a more ductile composite for the development of super infrastructure.

Author Contributions: Conceptualization, M.Z., S.E., Y.T. and R.A.G.L.; methodology, M.Z., S.E. and Y.T.; formal analysis, M.Z., S.E. and Y.T.; investigation, M.Z., S.E. and Y.T.; resources, M.Z., S.E., Y.T. and R.A.G.L.; data curation, M.Z. and S.E.; writing—original draft preparation, M.Z., S.E. and Y.T.; writing—review and editing, M.Z., S.E. and R.A.G.L.; visualization, M.Z., S.E. and Y.T.; supervision, R.A.G.L.; project administration, M.Z., S.E., Y.T. and R.A.G.L.; funding acquisition, R.A.G.L. All authors have read and agreed to the published version of the manuscript.

Funding: The authors wish to thank CEU San Pablo University Foundation for the funds dedicated to the project ref. MCP21V12 provided by CEU San Pablo University.

Institutional Review Board Statement: Not applicable.

Informed Consent Statement: Not applicable.

Data Availability Statement: The data presented in this study are available on request from the corresponding author.

Conflicts of Interest: The authors declare no conflict of interest.

References

1. Balapour, M.; Ramezanianpour, A.; Hajibandeh, E. An investigation on mechanical and durability properties of mortars containing nano and micro RHA. *Constr. Build. Mater.* **2017**, *132*, 470–477. [CrossRef]
2. Joshaghani, A.; Balapour, M.; Ramezanianpour, A.A. Effect of controlled environmental conditions on mechanical, microstructural and durability properties of cement mortar. *Constr. Build. Mater.* **2018**, *164*, 134–149. [CrossRef]
3. Joshaghani, A.; Moeini, M.A.; Balapour, M. Evaluation of incorporating metakaolin to evaluate durability and mechanical properties of concrete. *Adv. Concr. Constr.* **2017**, *5*, 183–199. [CrossRef]
4. Karein, S.M.M.; Balapour, M.; Karakouzian, M. Improving the hardened and transport properties of perlite incorporated mixture through different solutions: Surface area increase, nanosilica incorporation or both. *Constr. Build. Mater.* **2019**, *209*, 187–194. [CrossRef]
5. Ramezanianpour, A.; Ghoreishian, S.; Ahmadi, B.; Balapour, M.; Ramezanianpour, A. Modeling of chloride ions penetration in cracked concrete structures exposed to marine environments. *Struct. Concr.* **2018**, *19*. [CrossRef]
6. Balapour, M.; Joshaghani, A.; Althoey, F. Nano-SiO_2 contribution to mechanical, durability, fresh and microstructural characteristics of concrete: A review. *Constr. Build. Mater.* **2018**, *181*, 27–41. [CrossRef]
7. Balapour, M.; Zhao, W.; Garboczi, E.J.; Oo, N.Y.; Spatari, S.; Hsuan, Y.G.; Billen, P.; Farnam, Y. Potential use of lightweight aggregate (LWA) produced from bottom coal ash for internal curing of concrete systems. *Cem. Concr. Compos.* **2020**, *105*, 103428. [CrossRef]
8. Wang, X.Q.; Chow, C.L.; Lau, D. A review on modeling techniques of cementitious materials under different length scales: Development and future prospects. *Adv. Theory Simul.* **2019**, *2*, 1900047. [CrossRef]
9. Chae, S.R.; Moon, J.; Yoon, S.; Bae, S.; Levitz, P.; Winarski, R.; Monteiro, P.J.M. Advanced nanoscale characterization of cement based materials using X-ray synchrotron radiation: A review. *Int. J. Concr. Struct. Mater.* **2013**, *7*, 95–110. [CrossRef]
10. Ardalan, R.B.; Jamshidi, N.; Arabameri, H.; Joshaghani, A.; Mehrinejad, M.; Sharafi, P. Enhancing the permeability and abrasion resistance of concrete using colloidal nano-SiO_2 oxide and spraying nanosilicon practices. *Constr. Build. Mater.* **2017**, *146*, 128–135. [CrossRef]
11. Joshaghani, A.; Moeini, M.A. Evaluating the effects of sugar cane bagasse ash (SCBA) and nanosilica on the mechanical and durability properties of mortar. *Constr. Build. Mater.* **2017**, *152*, 818–831. [CrossRef]
12. Mukhopadhyay, A.K. Next-generation nano-based concrete construction products: A review. *Nanotechnol. Civ. Infrastruct.* **2011**, 207–223. [CrossRef]
13. Tosee, S.V.; Faridmehr, I.; Bedon, C.; Sadowski, Ł.; Aalimahmoody, N.; Nikoo, M.; Nowobilski, T. Metaheuristic Prediction of the Compressive Strength of Environmentally Friendly Concrete Modified with Eggshell Powder Using the Hybrid ANN-SFL Optimization Algorithm. *Materials* **2021**, *14*, 6172. [CrossRef] [PubMed]
14. Ziada, M.; Erdem, S.; Tammam, Y.; Kara, S.; Lezcano, R.A. The Effect of Basalt Fiber on Mechanical, Microstructural, and High-Temperature Properties of Fly Ash-Based and Basalt Powder Waste-Filled Sustainable Geopolymer Mortar. *Sustainability* **2021**, *13*, 12610. [CrossRef]
15. Sahmaran, M.; Lachemi, M.; Hossain, K.M.A.; Ranade, R.; Li, V.C. Influence of aggregate type and size on ductility and mechanical properties of engineered cementitious composites. *ACI Mater. J.* **2009**, *106*, 308.
16. Banthia, N.; Gupta, R. Influence of polypropylene fiber geometry on plastic shrinkage cracking in concrete. *Cem. Concr. Res.* **2006**, *36*, 1263–1267. [CrossRef]
17. Han, T.C.; Wang, F.J.; Dou, H.Q. Application of ultra high toughness cementitious composites to tunnel lining. *Appl. Mech. Mater.* **2013**, *256*, 1226–1229. [CrossRef]
18. Nyström, U.; Gylltoft, K. Comparative numerical studies of projectile impacts on plain and steel-fibre reinforced concrete. *Int. J. Impact Eng.* **2011**, *38*, 95–105. [CrossRef]
19. Cai, X.H.; He, Z.; Liu, W. Experimental study on Impact Resistance of PVA Fiber Reinforced Cement-based Composite. *Appl. Mech. Mater.* **2014**, *584*, 1630–1634. [CrossRef]
20. Manikandan, V.; Jappes, J.T.W.; Kumar, S.M.S.; Amuthakkannan, P. Investigation of the effect of surface modifications on the mechanical properties of basalt fibre reinforced polymer composites. *Compos. Part B Eng.* **2012**, *43*, 812–818. [CrossRef]
21. Jalal, A.; Shafiq, N.; Nikbakht, E.; Kumar, R.; Zahid, M. Mechanical properties of hybrid basalt-polyvinyl alcohol (PVA) fiber reinforced concrete. *Key Eng. Mater.* **2017**, *744*, 3–7. [CrossRef]
22. Chaipanich, A.; Nochaiya, T.; Wongkeo, W.; Torkittikul, P. Compressive strength and microstructure of carbon nanotubes–fly ash cement composites. *Mater. Sci. Eng. A* **2010**, *527*, 1063–1067. [CrossRef]
23. Luo, Z.; Li, W.; Gan, Y.; He, X.; Castel, A.; Sheng, D. Nanoindentation on micromechanical properties and microstructure of geopolymer with nano-SiO_2 and nano-TiO_2. *Cem. Concr. Compos.* **2021**, *117*, 103883. [CrossRef]
24. Li, V. On Engineered Cementitious Composites (ECC) A Review of the Material and Its Applications. *J. Adv. Concr. Technol.* **2011**, *1*, 215–230. [CrossRef]
25. Lepech, M.D.; Li, V.C. Large-scale processing of engineered cementitious composites. *ACI Mater. J.* **2008**, *105*, 358.
26. Li, V.C. *Engineered Cementitious Composites-Tailored Composites through Micromechanical Modeling, Fiber Reinforced Concrete*; Banthia, N., Bentur, A., Mufti, A., Eds.; Present and the Future, Canadian Society of Civil Engineers: Montreal, QC, Canada, 1997; p. 38.
27. Ekaputri, J.; Limantono, H.; Triwulan, T.; Susanto, T.; Abdullah, M.M.A.B. Effect of PVA Fiber in Increasing Mechanical Strength on Paste Containing Glass Powder. *Key Eng. Mater.* **2015**, *673*, 83–93. [CrossRef]

28. Kunieda, M.; Rokugo, K. Recent progress on HPFRCC in Japan. *J. Adv. Concr. Technol.* **2006**, *4*, 19–33. [CrossRef]
29. Li, V.C.; Wang, S.; Wu, C. Tensile strain-hardening behavior of polyvinyl alcohol engineered cementitious composite (PVA-ECC). *Mater. J.* **2001**, *98*, 483–492.
30. Ling, Y.; Zhang, P.; Wang, J.; Taylor, P.; Hu, S. Effects of nanoparticles on engineering performance of cementitious composites reinforced with PVA fibers. *Nanotechnol. Rev.* **2020**, *9*, 504–514. [CrossRef]
31. Topič, J.; Prošek, Z.; Indrová, K.; Plachý, T.; Nežerka, V.; Kopecky, L.; Tesarek, P. Effect of PVA modification on the properties of cement composites. *Acta Polytech.* **2015**, *55*, 64–75. [CrossRef]
32. Yan, H.; Ran, Q.; Yang, Y.; Shu, X.; Zhang, Q.; Zhang, J.; Liu, J. Investigation on the Effect of Hydroxyapatite Nanorod on Cement Hydration and Strength Development. *J. Nanosci. Nanotechnol.* **2021**, *21*, 1578–1589. [CrossRef] [PubMed]
33. Zhang, P.; Zheng, Y.; Wang, K.; Zhang, K. Combined influence of nano-$CaCO_3$ and polyvinyl alcohol fibers on fresh and mechanical performance of concrete incorporating fly ash. *Struct. Concr.* **2020**, *21*, 724–734. [CrossRef]
34. Ficker, T.; Martišek, D. Digital fracture surfaces and their roughness analysis: Applications to cement-based materials. *Cem. Concr. Res.* **2012**, *42*, 827–833. [CrossRef]
35. Ficker, T.; Martišek, D.; Jennings, H.M. Roughness of fracture surfaces and compressive strength of hydrated cement pastes. *Cem. Concr. Res.* **2010**, *40*, 947–955. [CrossRef]
36. Erdem, S.; Blankson, M.A. Fractal–fracture analysis and characterization of impact-fractured surfaces in different types of concrete using digital image analysis and 3D nanomap laser profilometery. *Constr. Build. Mater.* **2013**, *40*, 70–76. [CrossRef]
37. Farhan, A.H.; Dawson, A.R.; Thom, N.H. Characterization of rubberized cement bound aggregate mixtures using indirect tensile testing and fractal analysis. *Constr. Build. Mater.* **2016**, *105*, 94–102. [CrossRef]
38. Farina, I.; Goodall, R.; Hernández-Nava, E.; di Filippo, A.; Colangelo, F.; Fraternali, F. Design, microstructure and mechanical characterization of Ti6Al4V reinforcing elements for cement composites with fractal architecture. *Mater. Des.* **2019**, *172*, 107758. [CrossRef]
39. Ding, Y.; Liu, J.-P.; Bai, Y.-L. Linkage of multi-scale performances of nano-$CaCO_3$ modified ultra-high performance engineered cementitious composites (UHP-ECC). *Constr. Build. Mater.* **2020**, *234*, 117418. [CrossRef]
40. *ASTM C597*; Standard Test Method for Pulse Velocity Through Concrete. ASTM International: West Conshohocken, PA, USA, 2016.
41. *ASTM C109/C109M*; Standard Test Method for Compressive Strength of Hydraulic Cement Mortars (Using 2-in. or [50 mm] Cube Specimens). ASTM International: West Conshohocken, PA, USA, 2021.
42. *ASTM C230*; Standard Specification for Flow Table for Use in Tests of Hydraulic Cement. ASTM International: West Conshohocken, PA, USA, 2008.
43. *ASTM C348*; Standard Test Method for Flexural Strength of Hydraulic-Cement Mortars. ASTM International: West Conshohocken, PA, USA, 2021.
44. Erdem, S.; Gürbüz, E. Influence of microencapsulated phase change materials on the flexural behavior and micromechanical impact damage of hybrid fibre reinforced engineered cementitious composites. *Compos. Part B Eng.* **2019**, *166*, 633–644. [CrossRef]
45. Guo, L.-P.; Sun, W.; Zheng, K.-R.; Chen, H.-J.; Liu, B. Study on the flexural fatigue performance and fractal mechanism of concrete with high proportions of ground granulated blast-furnace slag. *Cem. Concr. Res.* **2007**, *37*, 242–250. [CrossRef]
46. Moon, J.; Oh, J.E.; Balonis, M.; Glasser, F.P.; Clark, S.M.; Monteiro, P.J.M. High pressure study of low compressibility tetracalcium aluminum carbonate hydrates 3CaO· Al2O3· $CaCO_3$· 11H_2O. *Cem. Concr. Res.* **2012**, *42*, 105–110. [CrossRef]
47. Lothenbach, B.; Le Saout, G.; Gallucci, E.; Scrivener, K. Influence of limestone on the hydration of Portland cements. *Cem. Concr. Res.* **2008**, *38*, 848–860. [CrossRef]
48. Ariyagounder, J.; Veerasamy, S. Experimental Investigation on the Strength, Durability and Corrosion Properties of Concrete by Partial Replacement of Cement with Nano-SiO_2, Nano-$CaCO_3$ and Nano-$Ca(OH)_2$. *Iran. J. Sci. Technol. Trans. Civ. Eng.* **2021**. [CrossRef]
49. Camiletti, J.; Soliman, A.M.; Nehdi, M.L. Effect of nano-calcium carbonate on early-age properties of ultra-high-performance concrete. *Mag. Concr. Res.* **2013**, *65*, 297–307. [CrossRef]
50. Adesina, A.; Das, S. Performance of engineered cementitious composites incorporating crumb rubber as aggregate. *Constr. Build. Mater.* **2021**, *274*, 122033. [CrossRef]
51. Sun, M.; Zhu, J.; Sun, T.; Chen, Y.; Li, X.; Yin, W.; Han, J. Multiple effects of nano-$CaCO_3$ and modified polyvinyl alcohol fiber on flexure–tension-resistant performance of engineered cementitious composites. *Constr. Build. Mater.* **2021**, *303*, 124426. [CrossRef]
52. Jastrzebski, Z.D.; Komanduri, R. The Nature and Properties of Engineering Materials. *J. Eng. Mater. Technol.* **1988**, *110*, 294. [CrossRef]
53. Low, N.M.P.; Beaudoin, J.J. The flexural toughness and ductility of portland cement-based binders reinforced with wollastonite micro-fibres. *Cem. Concr. Res.* **1994**, *24*, 250–258. [CrossRef]
54. Yeşilmen, S.; Al-Najjar, Y.; Balav, M.H.; Şahmaran, M.; Yıldırım, G.; Lachemi, M. Nano-modification to improve the ductility of cementitious composites. *Cem. Concr. Res.* **2015**, *76*, 170–179. [CrossRef]
55. Erdem, S.; Dawson, A.R.; Thom, N.H. Impact load-induced micro-structural damage and micro-structure associated mechanical response of concrete made with different surface roughness and porosity aggregates. *Cem. Concr. Res.* **2012**, *42*, 291–305. [CrossRef]

56. Ren, Z.; Liu, Y.; Yuan, L.; Luan, C.; Wang, J.; Cheng, X.; Zhou, Z. Optimizing the content of nano-SiO_2, nano-TiO_2 and nano-$CaCO_3$ in Portland cement paste by response surface methodology. *J. Build. Eng.* **2021**, *35*, 102073. [CrossRef]
57. Chen, Z.; Yang, Y.; Yao, Y. Effect of nanoparticles on quasi-static and dynamic mechanical properties of strain hardening cementitious composite. *Adv. Mech. Eng.* **2019**, *11*, 1687814019846776. [CrossRef]
58. Du, Q.; Cai, C.; Lv, J.; Wu, J.; Pan, T.; Zhou, J. Experimental Investigation on the Mechanical Properties and Microstructure of Basalt Fiber Reinforced Engineered Cementitious Composite. *Materials* **2020**, *13*, 3796. [CrossRef] [PubMed]